Measurement of Erosion in Agricultural Fields Using Monoscopic Photogrammetry

Shlomo ABERGEL, Sagi FILIN, and Naftali GOLDSHLEGER, Israel

Key words: Soil erosion, Photogrammetry, Homography, Agriculture, Gabor filters

SUMMARY

Erosion in agricultural fields damages cultivated land that consequently causes agricultural and economic damage. Therefore, monitoring changes in the amount of soil erosion is important for agricultural planning as well as for planning the use of different soil conservation systems. This paper describes a terrestrial photogrammetry model for measuring erosion amounts and estimating the change in volume of raised beds, resulting from irrigation or rainstorms in cultivated fields. The example is taken from ridged and furrowed fields on sandy to loam soils (Typic Rhodoxeralfs) in the coastal plain of Israel. Unlike existing methods that are labor intensive and error prone, the approach described here enables a high-level of automation and accuracy while making use of low-cost consumer cameras. Emphasis is placed on parameters for robustness of the model and on linear methods that do not require approximate parameters for the photogrammetric solution. Experiments show that accurate results can be achieved in estimating volume and erosion.

Measurement of Erosion in Agricultural Fields Using Monoscopic Photogrammetry

Shlomo ABERGEL, Sagi FILIN, and Naftali GOLDSHLEGER, Israel

1. INTRODUCTION

Soil erosion and surface runoff in agricultural fields cause significant damage by clogging surface drainage systems, flooding roads and other nearby infrastructures (Fig. 1). They lead to loss of fertile soil and damage to agricultural crops (see Agassi and Bradford, 1999). To quantify erosion and the application of the different treatments, means to measure soil loss are needed. The common methods that are used for such measurements are predominantly based on manual work in the field and on a subsequent lengthy and error prone processing stage back in the office. As a result they are hard to apply on a field scale and complicate the assessment of different treatments for soil loss reduction.

Erosion quantification methods can be classified into three categories: point based, profile based, and volume related. Point based measurements are mostly implemented by measuring the change in surface level via pegs that are inserted into the soil (Hudson, 2001). The common profile based methods are base on manual measurements via stakes that are lowered from an upper girder, where the depth of the stakes defines the profile height at the point (Fig. 2a). Toy et al. (2003) make note to application of linear laser scanners to the measurement of linear changes (see also Salvati et al., 2000), however as the authors report the actual application of such methodology is limited, expensive, and cannot be applied easily. Finally, volumetric measurements are mainly based on integration of volume from profiles, or by classical leveling techniques (see Hudson, 2001). On a large scale, surveying can be performed via photogrammetry or by airborne laser scanners. However, the accuracy that can be reached by those methods (decimeter level) and their spatial resolution are insufficient to record the microtopography in cultivated fields.

Using the conventional methods for agricultural fields presents a number of significant problems. Some require installation of instruments in the field and have an indirect impact on the erosion. Others are cumbersome and may lead to crude or erroneous measurements, while others provide partial measurements that do not represent the real erosion. As such, existing methods are neither accurate nor convenient (see Agassi and Bradford, 1999).

Realizing the limitations of the prevailing techniques, this paper presents a photogrammetric mensuration method that offers high level of automation in calculating profiles from a sequence of images. The profile measuring scheme leads to volume calculation of raised beds, and consecutive measurements lead to the calculation of erosion. As the paper shows, spatial characteristics and robust methods allow achieving high- to full- level of automation in estimating the volume. This allows acquiring image data without imposing constraints on the imaging process, and so enables non-experts to apply it to estimate volume. The

employed photogrammetric models do not require knowledge about the camera position or internal parameters and so enables the use of consumer cameras for this process, thus making it inexpensive to perform.

Fig. 1. A field after the erosion damage (left); the field was retilled (on the right).

Fig. 2. Profile meters, a) common profile-meter, b) the proposed measuring-frame.

2. VOLUME MEASUREMENT OF RAISED BEDS BASED ON TERRESTRIAL PHOTOGRAMMETRY

The proposed model makes use of a measuring-frame in the form presented in Fig. 2b. In principle, this frame may be classified as a profile meter, however contrary to the commonly used one (Fig. 2a), this instrument is not designed for physical profile measurement, but rather constitutes a reference frame. To define the profile, a strip of fabric is placed on the soil, next to the frame. The plane defined by the frame in object space constitutes the profile surface, while the white fabric expresses the profile itself. The frame and the fabric edge lie on a same plane and are then photographed (Fig. 2b). The volume of the raised beds is measured in stages. First, the profile areas along the beds are calculated and then integration is carried out to calculate the volume. It is noted that due to the relatively uniform surface texture of the beds, an effective use of a stereoscopy for direct evaluation of neither profiles nor the volume is possible. Therefore, a monoscopic solution that makes use of the fabric as a profile marker is the chosen option.

The computation of the profile along the bed requires an image-to-object space transformation. This transformation should take into account the absence of fixed internal camera parameters between images (this is true for consumer cameras), and the imaging from general locations. These two constraints lead to a difficulty in initializing the generally non-linear photogrammetric solution (Kraus, 1999). In order to handle a large number of images, the proposed model aims achieving the highest possible level of automation in profile evaluation, reducing the work into the data acquisition only. We present an approach that handles both problems. Calculation of the volume is based on estimating the profile areas from the collection of images. Estimation of the profile areas is made up of a number of intermediate stages: autonomous detection of the frame in image space, estimation of transformation from the image to the object-space profile surface, and autonomous detection of the profile and calculation of the area trapped under it.

3. AUTONOMOUS PROFILE EXTRACTION

The proposed model is based on identifying prominent points on the frame as reference for photogrammetric image registration. Fig. 2b shows that the most natural set is the black squares on the measuring tape for which frame ordinates can be readily measured. Their detection is based on a two-step process in which the first involves a crude identification of the frame within the image and a crude detection of the squares inside of it. The second stage involves then fine localization that is aimed to achieve an accurate registration.

As a first step in the coarse detection phase, the regions of interest within the frame are identified. Since these regions relate to the black squares (the ordinates color) within the frame, we begin by searching for candidate regions. Since black color relates to zero intensity in all the three RGB channels, we compute the *value* channel within the HSV transformation. Experiments with different approaches like mode seeking in the intensity histogram and others has shown that a strategy that seeks dark regions surrounded by bright ones manages finding the regions of interest with a small number of outlying regions (see Fig. 3b). Dark and bright are defined via a naive thresholding on the two ends of the value channel. The regions serve as candidate patches within which the form of the target may appear. Within each of these regions we match a template resembling the shape of the sought target. We seek the pixel that responds with the highest correlation value (see Eq. 1),

$$r_{\max} = \max_{i,j}\left\{ r_{ij} \,\middle|\, r_{ij} = \frac{\sum_m \sum_n (I_{mn} - \bar{I}) \cdot (T_{mn} - \bar{T})}{\sqrt{(\sum_m \sum_n (I_{mn} - \bar{I})^2) \cdot (\sum_m \sum_n ((T_{mn} - \bar{T})^2)}} > t \right\} \qquad (1)$$

with r, the correlation value, t, a threshold value, and i,j the pixels within the search region. If the maximal value within the correlation map is not strong enough, the candidate region is dismissed leaving only pixels that offer strong confidence in their relevance (Fig 3c).

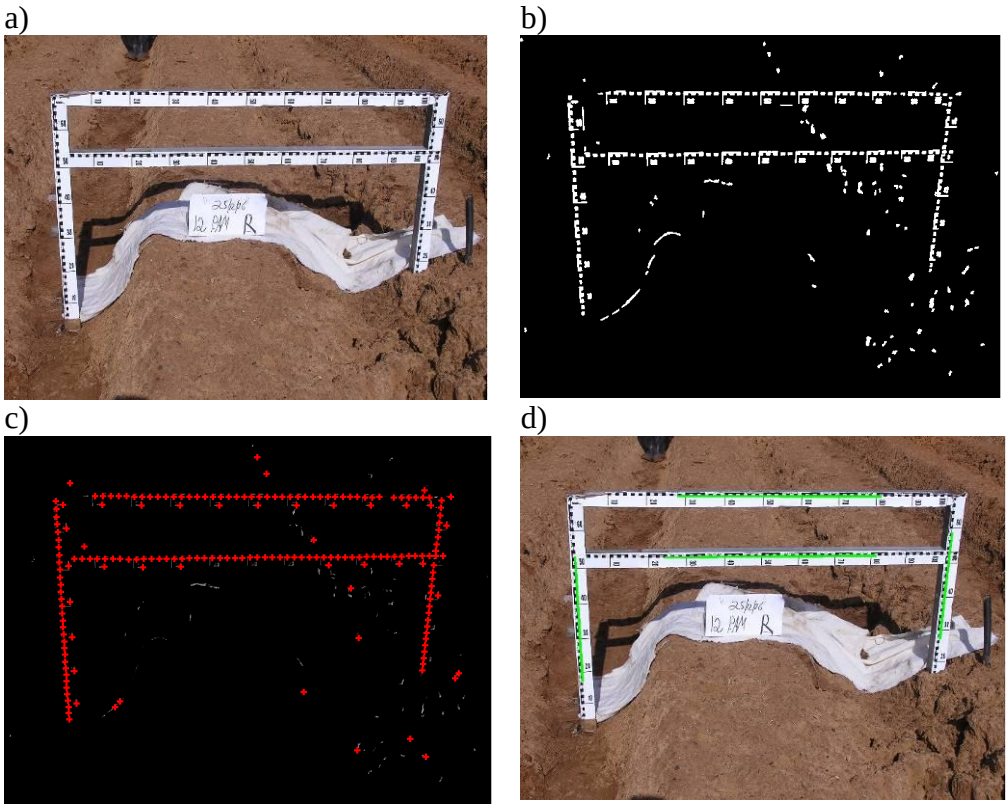

Fig. 3. The processing stages for the initial frame extraction, a) original image, b) candidate patches, c) correlation image (the highest values in red), d) four extracted lines (green).

3.1 Formation of Line Hypotheses

Some of the extracted points relate to the actual targets on the frame while others do not (see Fig. 3c). However, as the Figure shows many true responses exist. It is now left to separate the frame related points from the erroneous ones. While the Hough transformation has been applied for similar purposes; the dependency on cell parameters and the accuracy of the resulting lines, make its application more involved than what might seem first. We therefore recover the lines using the Random Sample Consensus (RANSAC) algorithm (Fischler and Bolles, 1981), an algorithm that is mainly applied for sets of observations in which some are inliers and others are outliers. We apply the algorithm until the four lines (composing the frame) have been detected.

The set of lines provides a set of candidates to launch a preliminary line homographic transformation given by

$$\mathbf{l}' = \mathbf{H}^{-T} \cdot \mathbf{l} \qquad (2)$$

With $\mathbf{l}'$ the line equation in object space given as $\mathbf{l}'=[a, b, c]^t$, $\mathbf{l}$, the line equation in image space, and $\mathbf{H}$ the homographic transformation that is given by a 3×3 matrix which is fixed up to a scaling factor. Each line provides two independent equations and therefore four lines are

sufficient to compute the homographic transformation. While this transformation is coarse and offers no degrees of freedom, it can localize accurately on the target.

3.2 Geometric Transformation from Image to Profile Object-Space

Definition of the coarse orientation provides the starting point for the precise computation of the transformation from image to object-space. We use the ordinates along the frame as control points (24 points in all). The approximate location of these points can be reached directly based on the homography we have computed. Precise localization of the control points coordinates is then achieved by estimating the normalized cross-correlation between a template and the frame (see Eq. (1)). To achieve precession and compensating for the projective transformation distortion (which changes as a function of position) we rectify the image and search there. This rectification is relatively fast and saves the need to handle the individual affine distortions per target point.

Both frame and the profile form a plane in space, and the projective transformation between both planes can be written as a point based homographic transformation, given by Eq. (3), in which the extracted points serve as control

$$\boldsymbol{u} = \mathbf{H} \cdot \boldsymbol{x} \qquad (3)$$

$\boldsymbol{u}=[x, y, 1]^t$ is the homogeneous coordinate vector in the frame reference system, and $\boldsymbol{x}$, the homogeneous coordinate vector in image space. Since each point provides two equations (as it is for lines) solving the eight unknowns in the transformation requires at least four points. Thus, the detection of 24 points produces 40 degrees of freedom in the solution. The linearity in the homography estimation and the inclusion of internal camera parameters (focal length, perspective center and distortions) frees the computation from an initial approximation of the camera pose and from knowledge of its internal parameters.

Fig. 4. Detected reference points – 24 points overall (marked by blue circles), all are inliers.

The quality of the points that were detected on the frame depends on the radiometric quality of the image as well as on the initial detection of the frame. Due to foreshortening, dirt or inaccurate extraction of some of the lines that define the frame edge, these extracted points can include outliers (mistaken detections) and lead to a wrong solution. In order to filter gross

errors, the estimation of the homography is guided here by the RANSAC algorithm. Experience with a great number of images showed that the RANSAC-based solution leads to convergence already for the first set of candidates. Fig. 4 presents the results of the detection. The precision achieved is ~ ±2 [mm].

3.3 Profile Extraction

Transformation from image to object-space measures, as defined by the frame, enables computing the profile area. Inconsistent illumination and shadowing can contribute difficulties into the detection, because the gradients resulting from shadows effect fall both on the fabric and the ground and create strong edge responses, ones that are more dominant than the fabric-to-ground edges. Therefore, applying standard edge detectors (e.g., Canny) will either result in noisy edges, and when strong smoothing is applied, the edge localization will be affected by the isotropic nature of the filter. We make use of the Gabor filters, which offer directionality, as a means for better extraction of edges. Gabor filters are bandpass filters which find application in feature extraction, texture analysis, and stereo (see Jenkin and Jepson, 1994; Weldon et al., 1996). Their impulse response is created by multiplying a Gaussian envelope function with a complex oscillation. Gabor (1946) showed that these elementary functions minimize the space (time)-uncertainty product. By extending these functions to two dimensions it is possible to create filters which are selective for orientation. The even-symmetric real component of the original 2D Gabor filter (as proposed by Jain and Farrokhnia, 1991) is given by,

$$g_{even}(x,y) = e^{-\frac{1}{2}\left(\frac{x'^2}{\sigma_x^2}+\frac{y'^2}{\sigma_y^2}\right)} \cdot \cos\left(\frac{2\pi x'}{T}\right) \qquad (4)$$

with, $x' = x\cdot\cos\vartheta + y\cdot\sin\vartheta$; $y' = -x\cdot\sin\vartheta + y\cdot\cos\vartheta$; σ_x, σ_y, the *std*. of the Gaussian envelope; T, the period of the wave; and ϑ, its orientation.

The best filters for our purpose are small and tight, and according to the profile pattern, we use filters in three different orientations: 45°, 90°, 135° (see example in Fig. 5).

a) 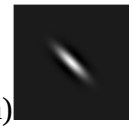 b) 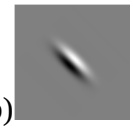

Fig. 5. An example of filters within our Gabor filter bank; a) an even filter with a 45° orientation, b) an odd filter with a 45° orientation.

The Gabor filters provide an amplitude image, which localizes on the sought target. We then extract the fabric boundary from the resulting gradient image. In shaded areas some discontinuities along the boundary may occur and will result in broken line fragments along the fabric boundary. We bridge these discontinuities by translating the edge-linking into a shortest-path problem, in which the local amplitude values serve as costs on the arcs. To minimize the computation complexity (as legitimate paths can be spanned all over the

image), we limit the search space into the gap zones along the profile and into a narrow band to around it.

As the profile defines a smooth and relatively simple curve (to the extent of the noise) it can be described by a low order polynomial curve. The fitting of the polynomial curve, whose degree should also be defined, should be robust to noise. The level of reliability of each point that is found is defined using a fitted polynomial (by using a confidence level α = 5%). In an iterative process, points whose difference from the function exceeds ΔL are deleted. A new polynomial is defined in each iteration by the remaining points and the threshold value, ΔL, is reduced. Fig. 6 demonstrates the entire process while filtering incorrect points. Polynomial degrees are usually between 4 and 7. As Fig. 6 shows, the polynomial adapted itself well to the profile line while eliminating noise influence by the fifteenth iteration.

The area enclosed underneath the profile can be computed using standard area calcualation equations (see Moffitt and Bossler, 1998). The accuracy estimates for the profile area are then derived via error propagation, and are given in Eq. (5)

$$m_A = \frac{\sqrt{\sum_1^n (y_{i+1} - y_{i-1})^2 + (x_{i+1} - x_{i-1})^2}}{2} m_x \qquad (5)$$

with m_x the accuracy estimate of point along the profile.

3.4. Volume Computation

Having the areas underneath the profiles computed, the volume of the raised beds is given by their integration. Since the number of vertices in each profile differs, the volumetric body that it form will be a prismatoid (Bradley, 1979), with *n* cross-sections.[1] The prismatoid volume is computed by an alternative form than the common one (Bradley, 1979) given by Eq. (6).

$$V = \frac{L}{2}\left(A_1 + A_n + 2\sum_2^{n-1} A_i \right) \qquad (6)$$

with, A_i, the profile area, and L, the distance between two profiles.
The volume accuracy is

$$m_V = \pm L\sqrt{(n - \frac{3}{2})} m_A \qquad (7)$$

[1] Note that the exact formula cannot be used here because the median cross-section that is formed between two cross-sections, cannot be computed as the number of vertices forming each section differs.

a)

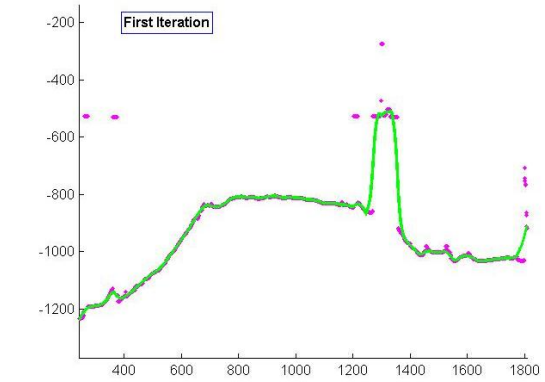

b)

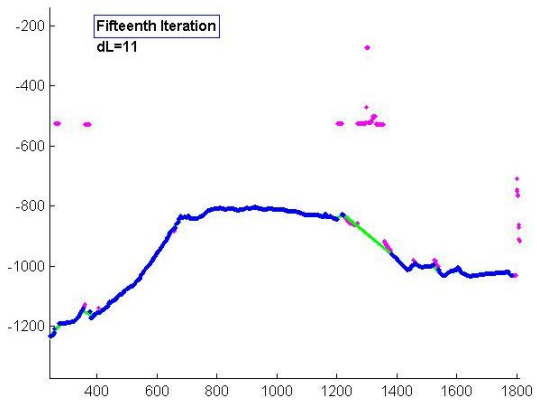

c)

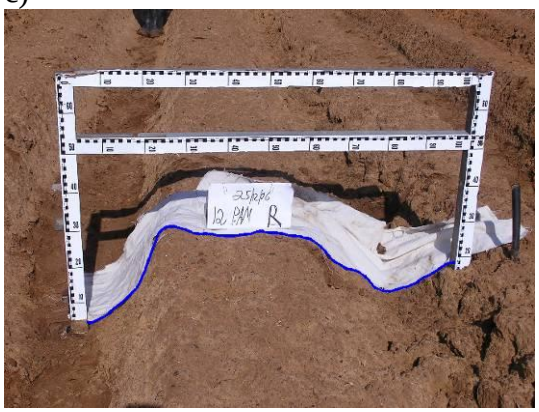

Fig. 6. The profile estimation, a, b) Iterative detection of the profile, based on a fixed fitted polynomial and the definition of its degree, (purple) – points detected as a profile, (green) – the fitted polynomial, (blue) – points compatible with polynomial, c) final extracted profile.

4. RESULTS AND DISCUSSION

The application of the overall process and the effect of the homographic transformation are demonstrated in Fig. 7, which shows the three stages of the process and the original image after being rectified into a front-looking view (the correction to the strong perspective distortion can readily be seen there). Notice that despite the strong distortion, the coarse detection has managed identifying correctly the frame and the targets inside, and that the fine localization has managed detecting all targets (marked in Fig. 7b by blue circles). In Fig. 7c the profile detection process is shown. It can be seen that the Gabor edges (green) managed localizing on the target but with some boundary problems. The robust estimation of the polynomial (shown in red and blue, as first and last iterations), which seeks smooth continuity, managed however removing it.

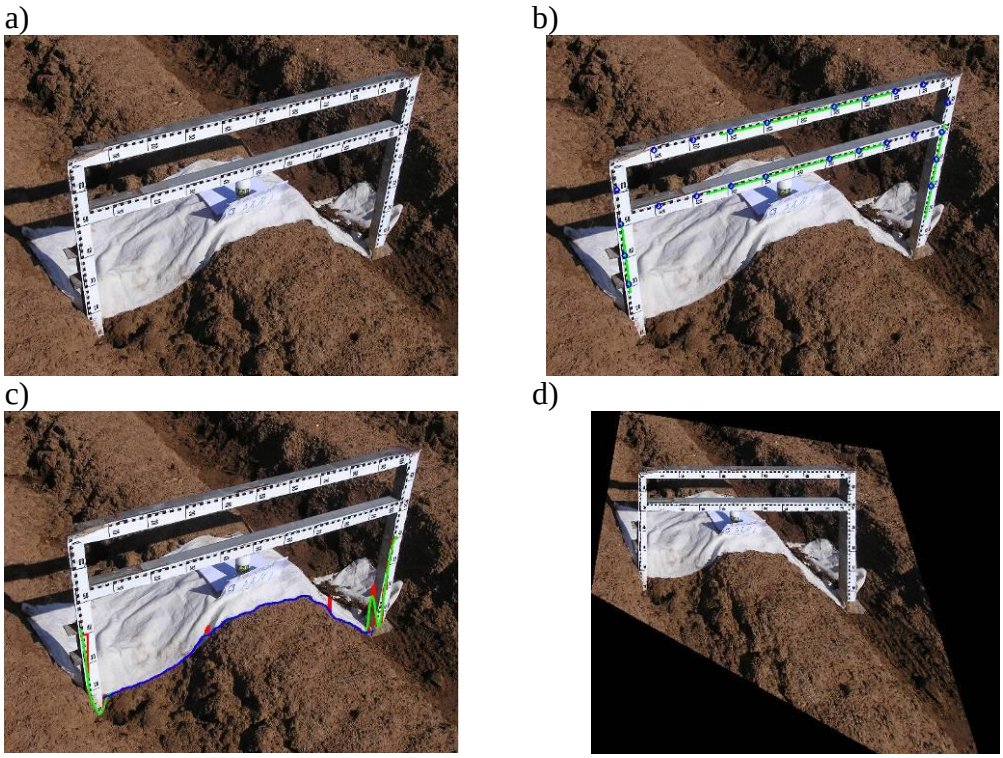

Fig. 7. The complete computation phase on an highly distorted image, a) the original image, b) the detection of the control information with green lines for the coarse stage and blue circles for the fine adjustment, c) the detection of the fabric (red) the original Gabor based detection, (green) the first fitted polynomial, and blue the final one, d) the frame after rectification into a front looking view.

To demonstrate of the robustness of the proposed model, we show in Fig. 8 results of extracting the same target from two images, taken with a relatively different viewing direction. The results show the extracted profile in its final form. The profiles are shown after transformation into the measuring-frame reference coordinate system and are overlaid together. One can see that the profiles were identified correctly the frame irrespective of the vantage point and scale (the photographer shadow can serve as an indication to that). The results in Fig. 8 show the ability to reconstruct the same contour shape without relying on the viewing direction. This means that no unique demands in the data acquisition phase are needed, while recovering similar results.

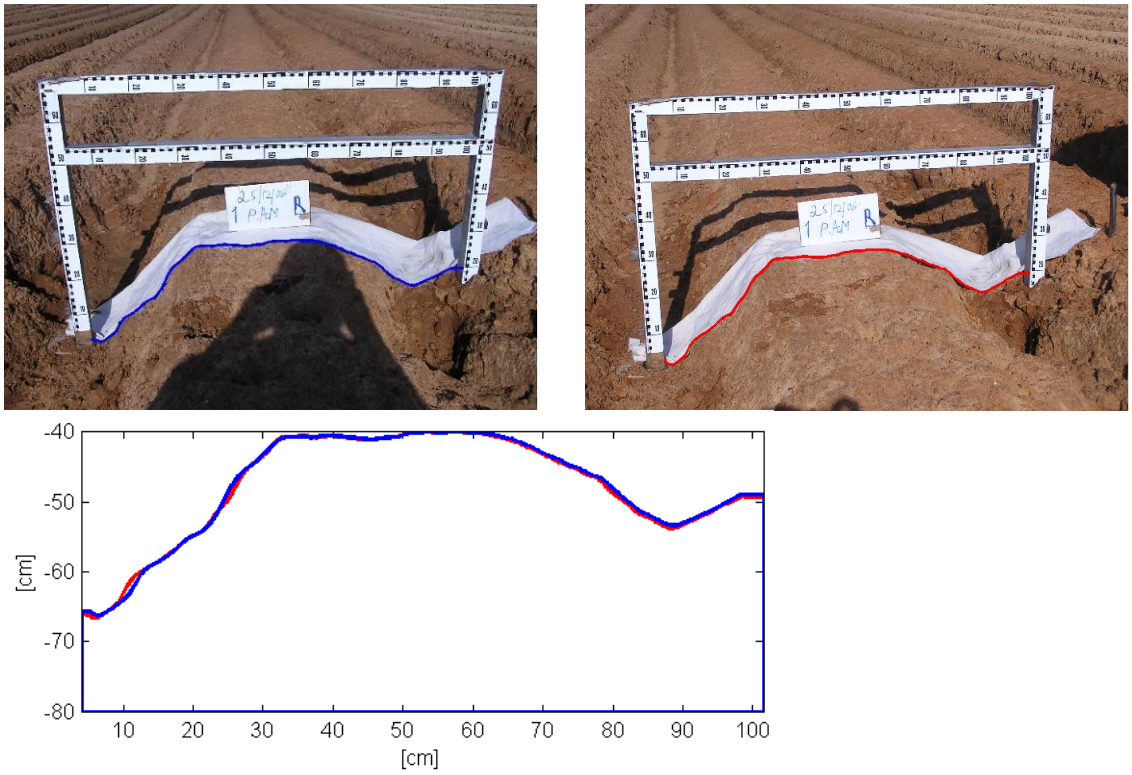

Fig. 7. An example of calculated profile from different images (top); the first image (blue) given 3145 [cm^2] and the second image (red) 3132 [cm^2]. The difference is of 13 [cm^2] over a100 [cm] long profile length. The mean difference is of 1.3[mm] only.

4.1 Application of the Volume Estimation for Treatment Analysis

The proposed model was applied, with comparison to conventional methods, in a trial carried out in a ridges furrowed field in Israel once in early winter before the beginning of the rainy season, and then right after a heavy rain storm. Two treatment systems were examined for reducing erosion damage – granular PolyAcrylaMide (PAM), and a gypsum and granular PAM mixture. Mixing PAM in the soil surface (Mamedov et al., 2007), or mixing PAM together with a source of electrolytes, such as gypsum, was found to be effective in controlling seal formation (e.g., Levy and Agassi, 1995; Tang et al., 2006). While application of PAM stops erosion it slightly reduces the water infiltration rate, the application of gypsum doubles the infiltration rate and also reduces erosion (Yu et al., 2003). The result of this phenomenon is increasing water infiltration and decreasing soil surface sealing and soil volume erosion (e.g. Levy et al., 1992; Ajwa and Trout, 2006).

Twelve raised beds were chosen, with each bed having seven transects measured at fixed distances of 10 [m]. These transects were marked by pegs that served as a control point for re-measuring after the rainy season. Four of the raised beds served as control, four were used for the PAM treatment and four were used for the gypsum and PAM mixture treatment. The profiles were imaged at each control point at the beginning and at the end of the rainy season. The sand displaced from the center of the profile, and the sand that accumulated at the sides

of the profile, were calculated separately when calculating erosion. The average precision received from the homography was ±0.18 [cm] and for confidence interval of 95% was ± 0.35 [cm]. Volume precision (with confidence interval of 95%) for a prismatoid with seven profiles that was received is: ±0.0017 [m^3]. Volume accuracy for a dunam unit (1,000 m^2) with confidence interval of 95% is: ±0.007 [m^3/dunam]. The accuracy estimates is a fraction of a percent of the calculated volume. Table 1 lists the soil loss volume as computed for the application of the different treatments. It generally shows that the usage of PAM, and especially gypsum with PAM in Hamra soil reduces the erosion. These results conform to independent measurements that were taken by using a mechanical profile meter. However, the ease of using the image based profile meter and the high-level of automation make it advantageous to the mechanical one.

Control		PAM		Gypsum + PAM	
Side	Center	Side	Center	Side	Center
8.68	-40.87	7.22	-19.19	19.90	-20.91

Table 1: Calculation of erosion values [m^3/dunam] (negative values – loss of soil; positive values - accumulation).

5. SUMMARY AND CONCLUSIONS

The paper presented an autonomous model to estimate the volume of raised beds and resulting estimate of erosion based on terrestrial photogrammetry. It can be seen that understanding the character of the problem and using models robust to noises enable autonomous photogrammetric solution of images, as well as an autonomous calculation of the profiles. The proposed model shows stability in calculation of transformation as well as in detecting the profile, even under relatively strong inclination angles. Such stability is important for creation of a solution that is accessible to end users with no photogrammetric background. The research presented a combination of relatively simple working methods in the field, with a high-level of automation, leading to an effective solution for this complex problem. The solution enables configurational analysis of the variables in raised bed profiles as a basis for analyzing erosion.

ACKNOWLEDGEMENTS

The research was funded in part by Ministry of Agriculture and Rural development.

REFERENCES

Agassi M., and Bradford, J.M., 1999. Methodologies for interrill soil erosion studies, Soil & Tillage Research 49 (1999) 277-287.

Ajwa, H.A., and T.J. Trout. 2006. Polyacrylamide and water quality effects on infiltration in sandy loam soils. Soil Sci. Soc. Am. J. 70:643–650.

Bradley A. D, 1979. Prismatoid, Prismoid, Generalized Prismoid. The American Math. Monthly, 86: 486-490.

Dan, Y., and Raz., Z., 1970, Soil association Map of Israel in Hebrew Volcani Institute for Agriculture Research, Beit Dagan Israel.

Fischler M.A., Bolles R.C., 1981. Random Sample Consensus: A paradigm for model fitting with application to image analysis and Automated Cartography. Communication Association and Computing Machine, 24(6), 381-395.

Gabor, D., 1946. Theory of communication. J. IEEE, 93: 429-457.

Hudson N. 2001. Soil Conservation. Itaca. N.Y. Cornell University Press.

Jain A.K. and Farrokhnia F., 1991. Unsupervised texture segmentation using Gabor filters. Pattern Recognition, 24: 12, 1167–1186.

Jenkin M. R. M., Jepson, A. D., 1994. Recovering Local Surface Structure through Local Phase Difference Measurements. Computer Vision, Graphics and Image Processing: Image Understanding, 59: no. 1, 72-93.

Kraus, K. 1999. Photogrammetry, Vol 1. 4th ed. Bonn, Germany: Dümmler.

Levy, G.J., and M. Agassi. 1995. Polymer molecular weight and degree of drying effects on infiltration and erosion of three different soils. Aust. J. Soil Res. 33:1007–1018.

Levy, G.J., J. Levin, M. Gal, M. Ben-Hur, and I. Shainberg. 1992. Polymers' effects on infiltration and soil erosion during consecutive simulated sprinkler irrigation. Soil Sci. Soc. Am. J. 56:902–907.

Mamedov A. I., Huang C., Beckmann S., 2007. Aggregate Stability as Affected by Polyacrylamide Molecular Weight, Soil Texture, and Water Quality SSSAJ, 71(6) , 1918- 1909

Moffitt, F., H., Bossler, J., 1998. Surveying. Addison-Wesley, Menlo Park, Calif.

Pellejero O., A., Sagüés, and J. J., Guerrero, 2004. Automatic Computation of the Fundamental Matrix from Matched Lines. R. Conejo et al. (Eds.): CAEPIA-TTIA, LNAI 3040. Springer-Verlag, Heidelberg. 197–206.

Salvati J. L., C. Huang, J. T. Johnson, and A. Klik, 2000. Soil Microtopography From The Soutern Great Plains Hydrology Experiments, 1999. In: Conference Proc. International Geoscience ans Remote Sensing Symposium (IGARSS, 2000), p. 1942-1944. IEEE publications, Piscatoway, NJ.

Tang, Z., J. Yu, T. Lei, I. Shainberg, A.I. Mamedov, and G.J. Levy. 2006. Runoff and erosion in sodic soils treated with dry PAM and phosphogypsum. Soil Sci. Soc. Am. J. 70:679–690.

Toy, T., Foster, G., R., Renard K., 2003. Soil Erosion: Processes, Prediction, Measurement, and Control. Wiley and Sons, Canada.

Weldon T., P., W., E. Higgins and D., E. Dunn, 1996. Efficient Gabor Filter Design For Texture Segmentation. Pattern Recognition, 29: No. 12, 2005-2015,

Yu, J., Lei T., Shainberg I., Mamedov A.I., and Levy G.J., 2003. Infiltration and erosion in soils treated with Dry PAM and gypsum. Soil Sci. Soc. Am. J., 67: 630-636.

BIOGRAPHICAL NOTES

Mr. Shlomo Abergel graduated form the Technion - Israel Institute of Technology in Mapping and Geo-Information Engineering in 2006. He is currently pursuing his MSc degree in Mapping and Geo-Information Engineering**.**

Dr. Sagi Filin graduated form the Technion - Israel Institute of Technology in Geodetic Engineering in 1989. In 1995 he received is M.Sc degree in Geodetic Engineering from the Technion and in 2001 his Ph.D. degree in Geodetic Sciences from The Ohio State University. From 2001 until 2004 he was with the Photogrammetry and Remote Sensing Section in Delft University of Technology. Since 2004 he is a faculty member in Civil and Environmental Engineering in the Department of Transportation and Geo-Information Engineering.

Dr. Naftali Goldshleger graduated form the Hebrew University in Geology in1975. In 1985 he received the M.Sc degree in Geophysics Sciences from The Tel-Aviv University and in 1997 the Ph.D. degree in Geophysics Sciences from The Bar-Ilan University. From 2000 until 2001 he was in post doctoral research fellow in the Tel-Aviv University in the Department of Geography and Human Environment. Since 1998 he is a works as a researcher at the Soil Erosion Research Station in the Ministry of Agriculture and Rural Development, Israel.

CONTACTS

Mr. Shlomo Abergel
Department of Transportation and Geo-Information Engineering
Faculty of Civil and Environmental Engineering
Technion – Israel Institute of Technology
Haifa 32000,
ISRAEL
Email: as@tx.technion.ac.il
Tel. + 972 4 829-3065
Fax: +972 4 829-5708

Dr. Sagi Filin
Department of Transportation and Geo-Information Engineering
Faculty of Civil and Environmental Engineering
Technion – Israel Institute of Technology
Haifa 32000,
ISRAEL
Email: filin@tx.technion.ac.il
Tel. + 972 4 829-5855
Fax: +972 4 829-5708

Dr. Naftali Goldshleger
Soil Erosion Research Station

Ministry of Agriculture and Rural Development,
ISRAEL
Email: naftalig@moag.gov.il
Tel. + 972 9 890-0404
Fax: +972 9 898-5563